On the Relationship Between Water Vapor over the oceans and Sea Surface Temperature

Graeme L. Stephens

Department of Atmospheric Science, Colorado State University, Fort Collins, CO 80523

Submitted J. Clim. June, revised Nov. 1989.

NAG5-1127

Abstract

Monthly mean precipitable water data obtained from passive microwave radiometry are correlated with the NMC blended sea surface temperature data. It is shown that the monthly mean water vapor content of the atmosphere above the oceans can generally be prescribed from the sea surface temperature with a standard deviation of 0.36 gcm^{-2}. The form of the relationship between precipitable water and sea surface temperature in the range $T_s > 18^oC$ also resembles that predicted from simple arguments based on the Clausius-Clapeyron relationship. The annual cycle of the globally integrated mass of SMMR water vapor is shown to differ from analyses of other water vapor data in both phase and amplitude and these differences point to a significant influence of the continents on water vapor. Regional scale analyses of water vapor demonstrate that monthly averaged water vapor data, when contrasted with the bulk sea surface temperature relationship developed in this study, reflect various known characteristics of the time mean large-scale circulation over the oceans. A water vapor parameter is introduced to highlight the effects of large-scale motion on atmospheric water vapor. Based on the magnitude of this parameter, it is shown that the effects of large-scale flow on precipitable water vapor are regionally dependent, but for the most part, the influence of circulation is generally less than about ±20% of the seasonal mean.

1. Introduction

The role of water in the energy budget of the climate system is a topic of growing interest within the climate research community and has been proposed as the basic theme of GEWEX. [1] At present, however, large uncertainties exist in the estimation of the various components of the global water budget and, consequently, in certain important components of the global atmospheric and oceanic energy budgets. We now recognize that the connections between global hydrology and the Earth's energy budget are crucial to the problem of climate change. For instance, the predicted global warming due to a CO_2 doubling with water vapor feedback is approximately twice the warming predicted without feedback (the so-called fixed relative humidity assumption of Manabe and Wetherald 1967). The distribution of water vapor, its transport, and divergence are also essential ingredients to our understanding of the distribution of solid and liquid water in the atmosphere and therefore crucial to the significant and perplexing problem of cloud feedback to climate change (e.g., Paltridge 1980; Sommerville and Remer 1984; Roeckner *et al.* 1987 and Stephens *et al.* 1989 among others).

Water vapor is also important to other physical processes that occur in the atmosphere. Water vapor plays a decisive role in the transfer of radiation through the atmosphere and is important to the transport and release of latent heat. The distribution of latent heat release is a topic that has received considerable attention over the past decade especially with the burgeoning interest in the variability of the atmosphere on both inter- and intra-seasonal time scales. More specifically, several studies appear in the recent literature on the topic of intraseasonal variability and most focus on the explicit coupling between hydrology and atmospheric dynamics. The results of Gill's (1982) study on moist dynamics, for example, provide insight into the role of moist processes in the physics of low frequency variability. Webster (1983) also noted the importance played by hydrological processes in a modeling study of monsoonal low frequency oscillations. Lau and Peng (1988) developed a self-consistent theory to explain intraseasonal oscillations of the tropical

[1] The Global Energy and Water Cyle Experiment (GEWEX) is a component of the World Climate Research Program.

atmosphere in which the effects of latent heating are parameterized directly as a function of the convergence of water vapor. In both that study and that of Gill (1982), explicit relationships between precipitable water vapor and sea surface temperature had to be assumed. Other studies (e.g., Emanuel 1987, and Neelin *et al.* 1987) have also alluded to the importance of evaporation from the warm ocean as a mechanism for sustaining low frequency oscillations of the tropical atmosphere.

These problems underscore the growing need to understand, at the very least, the bulk characteristics of the distribution of water vapor over the oceans, and in particular, its relationship to sea surface temperature. The importance of water vapor to a variety of atmospheric processes has been recognized for some time (e.g., Starr *et al.* 1969), but the poor coverage of conventional radiosonde data over the global oceans has both hindered our understanding of the distribution and transport of water vapor and at the same time highlighted the need for satellite-based measurements of water vapor. In response to this need, a number of different satellite approaches have been proposed over the past two decades to measure atmospheric water vapor. For instance, there have been several attempts to estimate water vapor using passive infrared techniques. Shen and Smith (1973) employed satellite infrared spectrometer radiation measurements (SIRS-B) taken from the Nimbus 4 satellite to estimate precipitable water. Retrieval of moisture fields from measurements made with the HIRS instrument on the Nimbus 6 and TIROS N satellites have been made by Hillger and Vonder Haar (1981) and Hayden *et al.* (1981). Prabhakara *et al.* (1979) used the high resolution spectral measurements obtained from the IRIS instrument flown on the Nimbus 4 satellite to study the distribution of precipitable water over the ocean. Perhaps most promising are techniques based on passive microwave remote sensing. For example, studies such as those of Staelin *et al.* (1976), Chang and Wilheit (1979), Grody *et al.* (1980), Njoku and Swanson (1984), Prabhakara *et al.* (1982, 1985), and Wentz (1983) among others have demonstrated the viability of microwave sensing of precipitable water over the world's oceans.

The aim of this study is to examine the relationship between monthly averaged precipitable water and sea surface temperature. The basic idea of relating precipitable water to surface mea-

surements is not new. For example, Reitan (1963), Smith (1966) and Viswanadham (1981) attempted to correlate precipitable water to surface due point temperature with ranging degrees of success. While these studies apply over land, Liu and Niiler (1984) and Liu (1986) considered the correlation of precitiable water to surface mixing ratio over the oceans in an attempt to derive an estimate of monthly mean latent heat flux at the ocean surface. In the present study, the precipitable water is correlated to the sea surface temperature. In general we expect this relationship to be complicated by the influence of both large scale atmospheric circulation features on the precitiable water as well as local processes that influence the relative difference between evaporation from and precipitation to the surface. Unlike the previously mentioned studies, the present study aims to provide some idea of the relative importance of large scale processes versus local effects on the monthly averaged water vapor over the oceans. The data sources used in this study are described in section 2 and a simple theoretical relationship between precipitable water and sea surface temperature is developed in section 3. Comparisons between the observed relationships and the theoretical relationship are presented in section 4 and departures from the bulk relationship are shown to identify large scale circulation influences on the water vapor.

2. Data Sources

The water vapor data used in the analyses described in this paper are those obtained from the Scanning Multichannel Microwave Radiometer (SMMR) measurements using an algorithm developed by Prabhakara *et al.* (1982) based on the measured brightness temperatures at 21 and 18 GHz. An advantage of their retrieval scheme, and one especially relevant to the desired goals of the research described here, lies in the formulation of the retrieval in terms of the difference of brightness temperature between two adjacent frequencies. By differencing these temperatures. the radiometric effects of sea surface emission, and thus any significant sea surface temperature biases in the data, are therefore minimized. Similarly, the effects of cloud water droplets and precipiation on the microwave emission and thus on the retrieved water vapor are largely mitigated by the difference between two adjacent frequencies. In an assessment of their retrieval approach.

Prabhakara *et al.* claim that the integrated water vapor content could be obtained with an *rms* error of about 0.25 $g.cm^{-2}$ based on comparison with radiosonde measurements of water vapor. This quoted error is similar to that estimated by Alishouse (1983) who used a different retrieval approach on SMMR measurements and is also comparable to the estimated error in precipitable water obtained from radiosonde data. The SMMR data used in this study are monthly averages and span a period of approximately five years[2] (January 1979 to September 1983) including the period of the much studied 1982-83 El Niño event. The data are grouped into rectangular areas 3° latitude by 5° longitude over the oceans from 75° N to 75° S. Figure 1 shows the 3×5 ocean grid on which the water vapor data are distributed. The data void blackened areas cover approximately 55% of the total global surface area. Because of the one day on, one day off cylce and the occasional missing or bad data, approximately 150 observations per month were obtained for each 3×5 grid box. Furthermore, the sun synchronous orbit of the Nimbus 7 provided for only two sets of observations each day that data were taken and the possibility of a diurnal bias in the data due to an inadequate sampling of the diurnal cycle cannot be ruled out.

The monthly averaged sea surface temperature (SST) data used here are part of the 2.5° global gridded SST data set produced operationally by the National Meteorological Center (NMC) by "blending" *in situ* and satellite observations. The *in situ* data consist of ship and buoy observations, and the satellite observations are obtained using multichannel SST techniques based on the AVHRR observations on the NOAA polar orbiting satellites (e.g., McClain *et al.* 1985). Because the first available month of these data is May 1979, a total of 52 months of concurrent SST and water vapor data were available for the analyses presented in this paper. The problems of NMC's SST analysis concerns the best way to blend the satellite and ship data sets to maximize the information in each. The method adopted at NMC was to use two days of *in situ* and satellite data to form the blended product (Gemmil and Larson 1979). These products were then averaged to

[2] *The reported comparison between radiosonde and retrieved water vapor were carried out systematically throughout the entire period. No appreciable effects of channel drift we evident in these comparisons. Prabhakara (personal communication).*

produce the monthly mean SST data used in this study. Unfortunately the two-day period chosen for the blending left significant areas of ocean undersampled and SST information for these areas tended to be weighted towards climatology. As a result, the data set for the time period that coincides with the SMMR data suffers from a tendency to smooth over SST anomalies (Gemmil, private communication). Recognition of these problems to a certain extent prompted NMC to undertake a modified analysis of SST observations by blending data collected over a period longer than 2 days (e.g., Reynolds 1988). Unfortunately, these improved SST data are not available for the SMMR time frame. However, the impact of these limitations on the analyses described below are likely to be relatively small given the interest of this study on climatological relationships between SST and water vapor.

A detailed discussion of water vapor distribution has been provided in earlier studies of Chang *et al.* (1984) and Prabhakara *et al.* (1985). The seasonal climatologies of the SMMR water vapor are well described by Prabhakara *et al.* (1985), and two examples are shown in Figs. 2a and 3a for the periods December to February (DJF) and June to August (JJA) averaged over the three non El Niño years. The respective climatologies of SST that match these global water vapor distributions are shown in Figs. 2b and 3b. A principal feature to note is the large area of atmospheric moisture greater than 5 gcm^{-2} over the equatorial Indian and western Pacific oceans (shaded area) which roughly corresponds to the pool of water warmer than about 29 ^{o}C (referred to as the Western Pacific warm pool). This is a persistent feature of both seasonal climatologies although the position and size of the moist air varies with season. Also of note are the regions of relatively low water vapor located over the eastern subtropical waters and associated with cold upwelling off the coasts of California, Chile, west Africa and Angola.

In contrast to these climatologies, water vapor and SST anomalies during May 1983, defined relative to the average of the three May months during the period 1979 to 1981, are shown in Figs. 4a and 4b respectively. A distinct feature of the water vapor anomaly distribution is the large area of positive anomaly (in excess of 1.2 gcm^{-2}) in the equatorial east Pacific associated with a warm SST anomaly in this region. Another obvious feature is the band of dry air across the Pacific that

branches out from the equatorial west Pacific eastward and northward into midlatitudes. A less extensive negative anomaly also occurs in the south Pacific off the coast of Chile.

The qualitative comparison of the anomaly fields provided by Figs. 4a and b reveals that a number of broadscale features of the water vapor anomaly are related to anomalies in SST. The negative water vapor anomalies just noted more or less match the negative SST anomalies. However, the correlation between water vapor and SST does not always hold. For instance, the area of negative SST anomaly in the equatorial west Pacific is not realized as a negative anomaly in water vapor. Furthermore, the area of positive SST anomaly in the eastern Pacific is less extensive than the positive water vapor anomaly in this region.

3. Analysis Procedure

Despite the complicating influences of both dynamics and thermodynamics on water vapor distribution, it is generally believed that its vertical distribution assumes a simple and predictable character. With this in mind, it is proposed that the vertical profile of specific humidity q has the form used previously for example by Smith (1966) and Sellers (1973) among others, namely

$$q = q_0 (p/p_o)^{\lambda} \tag{1}$$

where p is pressure and q_o, p_o are the respective surface values. The interpretation of λ is such that the scale height of water vapor is H/λ where H is the atmospheric scale height. If we take 7 km for a typical value of H and 2 km for the water vapor scale height, then a typical value of λ is 3.5.

It follows from the integration of (1) from $p = 0$ to $p = p_o$ that the precipitable water is

$$w = \frac{0.622}{g} \frac{e_o}{1+\lambda}. \tag{2}$$

where e_o in this expression is the surface vapor pressure

$$e_o = \frac{p_o q_o}{0.622} = r e_o^* \tag{3}$$

and r is the surface value of relative humidity. In (3), e_o^* is the saturation vapor pressure (in mb) which is determined from an approximation to the Clausius-Clapeyron equation of the form

$$e_o^* = 17.044 e^{a(T_s - 288)} \tag{4}$$

where T_s is the SST (Kelvin) and $a \approx 0.064(^oK)^{-1}$. From (2), (3), and (4), the relationship between precipitable water w (in gcm^{-2}) and sea surface temperature then follows as

$$w = 10.82 \left(\frac{r}{1+\lambda} \right) e^{a(T_s - 288)} \tag{5}$$

where the factor $r/1 + \lambda$ is deduced below by least squares fitting of SMMR derived values of w and the NMC SST's to (5). The relationship expressed by (5) is provided only as a convenient point of reference for the analysis of the observations described below and no claim is made that (5) actually represents the observed relationship between W and SST although it is shown that (5) fits the observations well for SST's in excess of 15^oC.

4. Results

(a) Global Relationships

Figures 5a and b provide graphical examples of the relationship between the seasonal means of SMMR derived precipitable water and SST averaged for the five June to August (JJA) seasons and the four December to February (DJF) seasons contained in the 52-month data set (upper panels). The points represented by open circles are the average of all observations that fall within a 1^oC temperature range centered about the given temperature. The extent of the shading above and below each of these average points represents the standard deviation for the data of each bin. Shown in the lower panel are the number of observations contained in the bin which were used to determine both the average and standard deviations. Apparent from both diagrams is the expected but dramatic increase in atmospheric water vapor as the SST is increased above about 20^oC. This feature is also apparent in Fig. 6 which shows the annually averaged relationship derived from the composite of all 52 months of data. The standard deviation of precipitable water

averaged over the range of SST's indicated on this diagram is $\pm 0.36\ gcm^{-2}$. The similarity of both seasons to the annually averaged relationship is further emphasized in Fig. 7. The mean DJF and JJA values are shown on this diagram together with the annual average relationship (solid curve). Also included for comparison are three examples of the relationship expressed by (5) with $r/(1+\lambda) = 0.1, 0.2$, and 0.3. The relationship between w and T_s, especially for $5 < T_s < 15$, is shown to differ from the simple expression derived from the Clausius-Clapeyron relationship using a single value of $r/(1+\lambda)$. The apparent increase of water vapor above that predicted from simple theory over this temperature range occurs at those latitudes marked by significant moisture convergence through meridional transports (e.g., Peixoto *et al.* 1978). However, for temperatures $T_s > 15°C$ a value of $r/(1+\lambda) = 0.162$ and $a = 0.0686$ in (5) provides a least squares fit to the data with a standard error of 4.8%.

Figure 8 presents time series of the monthly mean water vapor integrated over the SMMR ocean grid from $75°N$ to $75°S$ (upper panel), over the Northern Hemisphere (middle panel) and southern hemisphere (lower panel). The quantity represented by the dashed curve is the total integrated water vapor (in kg), or alternatively averaged precipitable water (in gcm^{-2}), and the averaged SST is given by the solid curves. The mass of water vapor over the global oceans has a mean of $7.2 \times 10^{15}\ kg$ which is 49% of the average mass of water vapor reported by Trenberth *et al.* (1987). The difference can largely be attributed to the reduced surface area coverage of the SMMR ocean grid compared to the full global data used by Trenberth *et al.* The annually averaged precipitable water derived from the SMMR data is $2.58\ gcm^{-2}$ which compares well with the values of $2.53\ gcm^{-2}$ and $2.57\ gcm^{-2}$ reported by Rosen *et al.* (1979) and Peixoto and Oort (1983) respectively, but is less than the $2.86\ g.cm^{-2}$ quoted by Trenberth *et al.*[3] although those authors admit to the possibility of a slight high bias in their data.

Whereas the mean SMMR precipitable water reasonably agrees with previously determined amounts, the amplitude of the annual cycles derived over the oceans of each hemisphere disagrees

[3] *The value derived from the ECMWF analyses has recently been revised to* $2.55\ gcm^{-2}$, *J.Christy (personal communication).*

with the hemispheric cycles deduced from global data. The amplitude of the annual cycle deduced from SMMR data is large and approximately 30% of the average value of the precipitable water over the repective oceans of both hemispheres. These cycles largely cancel to produce an annual cycle for water vapor over the global oceans that is significantly smaller in amplitude than for either hemisphere. These results are in direct contrast to those of Trenberth *et al.* who find an amplitude in both the global and hemispheric averaged water vapor that is approximately twice that shown in Fig. 8. The maximum of global SMMR precipitable water over the oceans peaks around April and is dominated by the annual cycle of water vapor over the southern oceans in contrast to the data of Trenberth *et al.*, who find maxima in the middle of the year in phase with the solar cycle over the Northern Hemisphere. While it is possible to suspect the representativeness of the Trenberth *et al.* data over the oceans as a cause for these differences, the differences in the annual cycle of water vapor over the oceans compared to that derived over the globe are likely to be real and thus point to a significant influence of the continents on global water vapor.

The sea surface temperatures averaged over the SMMR water vapor grid show the world oceans to be warmer in April, at the end of the solar heating period, than in October, at the end of the cooling period. This result is consistent with the oceanic temperature records of Levitus (1982) although the amplitude is somewhat more accentuated. The results suggest that the seasonal variation of water vapor over the world oceans reflects the seasonal changes in the global SST.

(b) Regional Relationships

While it is shown that the monthly mean water vapor over the oceans is, on the whole, a well behaved function of SST, important deviations from this general relationship occur on the regional scale. A number of important phenomena might produce regional scale departures in the gross relationship described above. For example, low level moisture convergence such as occurs in the vicinity of the ITCZ will produce regions of above average moisture. Also advection of moist air into a relatively dry region can also act to enhance the precipitable water of that region. On the other hand, advection of dry, cold air produces a drier than average atmosphere as do regions

of prevailing subsidence, such as within the trade wind regimes where dry air exists above an inversion. Thus significant deviations of precipitable water from that expected from the simple SST relationship reflect these large-scale processes.

To examine these excursions further, time series of water vapor and SST averaged over seven regions were studied. The regions chosen are labelled A through G in Fig. 9 for further reference. Figure 10 presents time series of monthly mean SMMR water vapor (solid curves) and SST (dashed curves) for each region. The comparisons reveal that the annual cycle of water vapor on a regional scale generally correlates with the annual cycle of SST except in the western Pacific (region B). There is also the suggestion that the annual cycle of water vapor in the equatorial and warm water regions (A, B, D and F) leads the annual cycle of SST in those regions. Of special note is the significant drying that occurs in region B during the first few months of 1983 and the related moistening of the eastern Pacific (region D) during the same period. These deviations from the normal water vapor content occur during the El Niño-Southern Oscillation episode and are consistent with our present understanding of that phenomenon. The deep convection normally located over region B and associated with the ascending branch of the Walker circulation shifts to the eastern Pacific over the anomalous warm water in that region and is replaced by large-scale subsidence (e.g., Webster, 1987). This subsidence produces a warming and drying of the middle troposphere above a lower, humid boundary layer thereby indicating a large-scale dynamical influence on atmospheric water vapor.

Figure 11 compares time series of the observed and predicted water vapor for the same seven regions and is presented to emphasize the differences between observed monthly mean water vapor and values predicted from the gross relationship between water vapor and SST derived from Fig. 6. The solid, heavy curve is the time series of monthly mean SMMR observations shown in Fig. 10 and the thin line is the water vapor deduced from interpolation of the data contained in Fig. 6. The extent of the shading about this thin line represents one standard deviation of water vapor above and below this predicted amount and is again determined by interpolation from Fig. 6. The observed water vapor amounts generally fall within this range for the seven selected regions, and

the predicted annual cycles of the water vapor reasonably match those observed in regions A, F, and G. However, there are notable and important deviations that exist between the observed and predicted water vapor amounts that suggest an influence of large-scale processes. For example, the effects of moisture advection are seen in regions C and D. The systematic difference between the observed and predicted water vapor amounts in the east Pacific region (D) is due to the influence of low level advection of moisture from the Caribbean Sea into the equatorial eastern Pacific. The significant moistening of region C during the boreal summer season can be attributed to eastward advection of moist air that originates from the moister regions of the western Pacific associated with the warm Kuroshio current and transported eastward along the northern flank of the subtropical high. The observed water vapor amounts in region B also tend to be larger than predicted during the boreal summer season especially during 1980 although this enhancement seems to undergo a marked interannual variability. The moistening of the western Pacific region can be related to the increased moisture convergence associated with the Asian monsoon. Other large-scale influences on water vapor distribution are evident in region E in which the enhanced wintertime drying relates to the large-scale subsidence associated with the accelerating equatorial flow along the eastern flank of the subtropical anticyclones. This explanation is also consistent with the vertical motion analysis of Oort (1983) who shows this subsidence to be strongest during the winter season in this region.

Following the work of Prabhakara *et al.* (1979), the parameter $(w - \bar{w})/w$ is introduced to highlight the effects of large-scale motion on atmospheric water vapor. In the definition of this parameter, w is the observed precipitable water and $\bar{w}$ is the value estimated given the SST and the relationship graphically portrayed in Fig. 6. Thus regions influenced by moisture convergence and/or moist air advection are characterized by positive values of this parameter whereas regions characterized by negative values suggest the influence of subsidence or dry air advection on water vapor. Because water vapor is concentrated in the first few kilometers above the ocean surface, the distribution of $(w - \bar{w})/w$ also indicates, in a gross way, the spatial configuration of the maritime

boundary layer (Prabhakara *et al.* 1979) and the magnitude of this quantity also indicates the quantitative effects of large scale circulation on precipitable water.

Figures 12a and b present the global distribution of $(w - \bar{w})/w$ derived for the DJF and JJA seasons respectively. The values of this quantity, expressed in Figs. 12 a and b as a percentage, vary from around -60% to $+20\%$ with large areas over the oceans ranging from $\pm 20\%$. Features that appear on these maps reflect various characteristics of the seasonal mean large scale circulation over the oceans.For instance, the areas of large scale subsidence associated both with regions of cold upwelling and of large scale subsidence along the eastern branches of the subtropical anticyclonic circulation over the North and South Pacific and Atlantic oceans are indicated by negative values of $(w - \bar{w})/w$. Positive values of this factor are found in the equatorial regions where moisture convergence associated with the ITCZ prevails. Some other outstanding features of these maps are the regions of almost continuous negative values of $(w - \bar{w})/w$ found during JJA in the Southern Hemisphere west of the date line between about $20^o - 30^o$S. The location of this region broadly agrees with the vertical motion fields calculated by Oort (1983) and is associated with the descending branch of the Hadley circulation. The relatively moist air over the North Pacific in JJA is also consistent with the large northward flux of moisture by transient eddies which is thought to occur in this region. A dominant feature of the DJF map is the dry air east of Japan and a similar but weaker dry feature east of the North American continent. These features are respectively associated with the climatological strong high pressure system located in the higher middle latitudes over the cold Eurasian continent and a weaker, less extensive high pressure system over Northern America. The dry air perhaps results from a combination of strong descent over the eastern portions of these pressure systems which extends eastwards over the Pacific and Atlantic oceans and the advection of dry air from the cold land mass over the warmer waters of these oceans. The existence of these dry areas is also consistent with the large latent and sensible heat releases that are perceived to occur in these regions (Budyko 1982). Both the seasonal and regional variability of $(w - \bar{w})/w$, evident for example off the east coasts of the Asian and north American

continents, may perhaps explain why other studies that attempt to correlate precipitable water to surface parameters show varying degrees of success (e.g., Viswanadham 1981).

5. Summary and Conclusions

A bulk relationship between monthly mean atmospheric precipitable water and sea surface temperature was established using 52 months of SMMR microwave water vapor data and monthly averaged NMC blended SST analyses. It was shown that a composite relationship between precipitable water and SST resembled that derived using simple thermodynamical arguments when the sea surface temperature exceeds about $15^{o}C$. It was also demonstrated that the annually averaged mass of water vapor integrated over the global oceans deduced from the SMMR observations are in reasonable agreement with certain previous estimates. However, both the phase and amplitude of the annual cycle of water vapor derived from SMMR, when integrated either over the global oceans or individually over the oceans of the Southern or Northern Hemisphere, deviate significantly from some previous findings. The study of Trenberth *et al.* (1987), for example, determine the amplitude of both the global and hemispheric averaged water vapor to be approximately twice that found in the SMMR data after differences in spatial coverage of the data are taken into consideration. The maximum in the annual cycle of global SMMR water vapor over the oceans peaks around April and is dominated by the annual cycle over the southern oceans in contrast to the data of Trenberth *et al.* which yield a maxima in the middle of the year in phase with the solar cycle over the Northern Hemisphere.

Analyses of the SMMR water vapor on a regional scale showed that the local departures of the observed precipitable water from that predicted from SST could be used as a tracer of large scale circulation. Regions of large scale subsidence associated with the mean meridional circulation and with the circulation about the subtropical anticyclones were clearly evident, as were the regions of moisture convergence associated with the ITCZ and transient eddy activity in the midlatitudes.

The basic conclusions that can be drawn from this study are as follows:

(i) The monthly mean water vapor content in the atmosphere above the oceans can generally be prescribed from the SST with an averaged standard deviation of 0.36 gcm^{-2}. The form of the relationship between precipitable water and SST surface temperature in the range $T_s > 15°C$ also resembles that predicted from simple arguments based on the Clausius-Clapeyron relationship. For these temperatures a value of $r/(1+\lambda) = 0.162$ and $a = 0.0686$ in (5) provides a least squares fit to the data with a standard error of 4.8%.

(ii) The annual cycle of the globally integrated mass of water vapor from SMMR over the oceans differs from other analyses in both phase and amplitude. It is possible that these differences are real and perhaps point to ocean-land differences in water vapor with a possible significant influence of the continents on global water vapor.

(iii) Monthly averaged water vapor data (denoted as w), when contrasted with the bulk SST relationship developed in this study (denoted as $\bar{w}$), were shown to reflect various known characteristics of the time mean large scale circulation over the oceans. The parameter $(w - \bar{w})/w$ was introduced both to highlight the effects of large scale motion on water vapor and to provide some quantitative measure of these effects on the seasonal mean water vapor. Based on the magnitude of this parameter, it was shown that the effects of large-scale flow on precipitable water vapor over the oceans is regionally dependent and, for the most part, the influence of circulation is generally less than about $\pm 20\%$ of the seasonal mean.

The analyses contained in this paper, both in terms of the bulk relationship between atmospheric water vapor and SST and the relationship between water vapor and the large scale circulation of the atmosphere, will hopefully provide a useful framework for comparisons between observed water vapor and that predicted by atmospheric general circulation models. For instance, it would be useful in the context of water vapor feedback in climate simulations to compare the correlation between the modeled precipitable water and sea surface temperature with the correlation found in this study. It is further hoped that comparisons of this type might provide insight into the behavior of water vapor in the atmosphere and point to improvements in our ability to model this behavior.

6. Acknowledgements

I gratefully acknowledge the kindness of C. Prabakhara for supplying me with the SMMR data. I also acknowledge the programming and graphics work of T. Greenwald. This work was partially supported by NASA Grant #NAG 5-1122

7. References

Alihouse,J.C., 1983:Total precipitable water and rainfall determinations from the SEASAT scanning multichannel microwave radiometer, *J.Geophys.Res.*,**88**, 1929-1935.

Budyko, M. I., 1982: *The Earth's Climate: Past and Future.* Academic Press, NY., 307pp.

Chang, A. T. C. and T. T. Wilheit, 1979: Remote sensing of atmospheric water vapor, liquid water and wind speed at the ocean surface by passive microwave techniques from NIMBUS 5 satellite. *Radio Sci.*, **14**, 793-803.

Emanuel, K. A., 1987: An air-sea interaction model of intraseasonal oscillations in the tropics. *J.Atmos. Sci.*, 44, 2324-2340.

Gemmil, W. and S. Larson, 1979: Real-time ocean thermal structure analysis. In: Papers submitted to the Joint IOC/WMO Seminar on oceanographic products and the IGOSS data processing system, Moscow, 1979.

Gill, A. E., 1982: Studies of moisture effects in simple atmospheric models: stable case. *Geophys. Astrophys. Fluid Dynamics*, **19**, 119-152.

Grody, N. C., 1976: Remote sensing of atmospheric water content from satellites using microwave radiometry. *IEEE Trans. Antennas. Propag.*, AP-24, 155-162.

Hayden, C. M., W. L. Smith and H. M. Woolf, 1981: Determination of moisture from NOAA polar orbiting satellite sounding radiances. *J. Appl. Met.* **20**, 450-466.

Hillger, D. W. and T. H. Vonder Haar, 1981: Retrieval and of high resolution moisture and stability fields from Nimbus 6 HIRS radiances in pre-convective situations. *Mon. Wea. Rev.*, **109**. 1788-1806.

Levitus, S., 1982: Climatological Atlas of the World Oceans. NOAA Prof. Paper No. 13, US Government printing office, Washington D.C., 173 pp.,NTIS PB83- 184093.

Liu,W.T., 1986:Statistical relation between monthly mean precipitable water and surface level humidity over global oceans.*Mon. Wea. Rev.*,**114**,1591-1602.

Liu,W.T. and P.P.Niiler, 1984: Determination of monthly mean humidity in the atmospheric surface layer over oceans from satellite data, *J.Phys.Oceanogr.*,**14**,1451-1457.

Manabe, S. and R. T. Wetherald, 1967: Thermal equilibrium of the atmosphere with a given distribution of relative humidity. *J. Atmos. Sci.*, **24**, 241-259.

McClain, E. P., W. G. Pichel and C. C. Walton, 1985: Comparative performance of AVHRR-based multichannel sea surface temperature. *J. Geophys. Res.*, **90**, 11587-11601.

Neelin, J. D., I. M. Held and K. H. Cook, 1987: Evaporation-wind feedback and low frequency variability in the tropical atmosphere. *J. Atmos. Sci.*, **44**, 2341-2348.

Njoku, E. G. and L. Swanson, 1983: Global Measurements of Sea Surface Temperature, Wind Speed and Atmospheric Water Content from Satellite Microwave Radiometer. *Mon. Wea. Rev.*, *111*, 1977-1987.

Oort, A. H., 1983: Global Atmospheric Circulation Statistics, 1958-1973. NOAA Professional Paper No.14, Rockville, Md., 180pp,NTIS PB84-129717.

Paltridge, G. W., 1980: Cloud-radiation feedback to climate. *Q. J. R. Meterol. Soc.*, **106**, 895-899.

Peixoto, J. P., R. D. Rosen and D. A. Salstein, 1978: Seasonal variability in the Pole to Pole modes of water vapor during IGY. *Arch. Met. Geophy. Biokl.*, Ser. A, **27**, 233-255.

Peixoto, J. P. and A. H. Oort, 1983: The atmospheric branch of the hydrological cycle and climate. in *Variations in the Global Water Budget*, D. Riedel, Hingham, Mass, 5-65.

Prabhakara, C., G. Dalu, R. C. Lo and N. R. Nath, 1979: Remote sensing of seasonal distribution of precipitable water vapor over the oceans and the inference of boundary layer structure. *Mon. Wea. Rev.*, **107**, 1388- 1401.

Reitan,G.H., 1963:Surface dew-point and water vapor aloft, *J.Appl.Meteor.*,**2**, 776-779.

Prabhakara, C., H. D. Chang and A. T. C. Chang, 1982: Remote sensing of precipitable water over the oceans from NIMBUS 7 microwave measurements. *J. Appl. Meteorol.*, **21**, 59-68.

Prabhakara, C., D. A. Short and B. E. Vollmer, 1985; El Niño and Atmospheric Water Vapor: Observations from Nimbus 7 SMMR. *J.C. Appl. Met.*, **24**, 1311-1324.

Reynolds, R. W., 1988: A real-time global sea surface temperature analysis. *J. Climate*, 1, 75-86.

Roeckner E., U. Schlese, J. Biercamp and P. Loewe, 1987: Cloud optical depth feedback and climate modeling. *Nature*, 138-140.

Rosen, R. D., D. A. Salstein and J. P. Peixoto, 1979: Variability in the annual fields of large scale atmospheric water vapor transport. *Mon. Wea. Rev.*, **107**, 26-37.

Sellers, W. D., 1973: A new global climatic model. *J.Appl.Met.*, **12**, 241-254.

Shen, W. C. and W. L. Smith, 1973: Statistical estimation of precipitable water with SIRS-B water vapor radiation measurements. *Mon. Wea. Rev.*, **101**, 24-32.

Smith, W. L., 1966: Note on the Relationship between total precipitable water and surface dew point. *J. Appl. Met.*, **5**, 726-727.

Sommerville, R. C. and L. A. Remer, 1984: Cloud optical thickness feedbacks in the CO_2 Climate Problem. *J. Geophys. Res.*, **89**, 9668-9672.

Staelin, D. H., K. F. Kunzi, R. L. Pettyjohn, R. K. L. Poon, R. W. Wilcox and J. W. Waters, 1976: Remote sensing of atmospheric water vapor and liquid water with the NIMBUS 5 microwave spectrometer, *J.Appl.Met.*,**15**,1204-1214.

Starr, V. P., Peixoto, J. P. and R. G. McKean, 1969: Pole-to-pole moisture conditions for the IGY. *Pure and Appl. Geophys.*, **75**, 300-331.

Stephens, G. L., P. W. Stackhouse, Jr., and P. J. Flatau, 1989: The relevance of the microphysical and radiative properties of cirrus clouds to climate and climatic feedback. In press, *J. Atmos. Sci.*, Feb. 1989.

Trenberth, K. E., J. R. Christy and J. G. Ohlsen, 1987: Global atmospheric mass, surface pressure, and water vapor variations. *J.Geophys.Res.*, **12**, 14815-14826.

Viswanadham,V.,1981: The relationship between total precipitable water and surface dew point. *J.Appl.Meteorol.*,**20**,3-8.

Webster, P. J., 1983: Mechanisms of monsoon low-frequency variability: Surface hydrological effects. *J. Atmos. Sci.*, **40**, 2110-2124.

Webster, P. J., 1987: The variable and interactive monsoon. *Monsoon*, Eds. Fein and Stephens, John Wiley and Sons, 269-330.

Wentz, F.J., 1983: A model function for ocean brightness temperatures. *J.Geophys.Res.*, **88**, C3, 1892-1906.

8. Captions to diagrams

Figure 1. Map portraying the ocean grid used in the analysis of SMMR water vapor data. The data void areas (blackened) lie over major land masses and islands.

Figure 2a. The climatological distribution of SMMR precipitable water obtained as an average of the three DJF seasons for the years indicated. Contours have units of gcm^{-2}.

Figure 2b. The climatological distribution of SST obtained as an average of the same DJF seasons used to obtain Fig. 2a. Contours have units of ^{o}C. The warm pool regions exceeding $28^{o}C$ are highlighted.

Figure 3a. Same as Fig. 2a but for the three JJA seasons of the years indicated.

Figure 3b. Same as Fig. 2b but for JJA.

Figure 4a. The May 1983 precipitable water anomaly distribution (contours have units of gcm^{-2}).

Figure 4b. The May 1983 SST anomaly field (^{o}C).

Figures 5a and b. Graphical representations of the relationship between precipitable water and SST (upper panels) obtained from the composite of all (a) DJF and (b) JJA seasons contained in the data set. The shading above and below each point is one standard deviation above and below the averaged data point. The number of observations used to form this average and standard deviation are shown as histograms in the lower panel.

Figure 6. Same as Figs 5a and b but for the annual mean.

Figure 7. The annually averaged relationship extracted from Fig. 6 (heavy solid line) compared to the DJF and JJA values from Figs. 5a and b (symbols). Three examples of the Clausius-Clapeyron expression (5) are also shown for the stated values of $r/(1+\lambda)$.

Figure 8. Time series of SST (solid) and precipitable water (dashed) averaged over the ocean SMMR grid shown in Fig 1. The upper panel applies to the average over the entire ocean grid, the middle panel to the NH and the lower panel to the SH. The water vapor is also expressed in units of total water vapor mass (kg and righthand-most scale).

Figure 9. The location of the seven regions (referenced by A through G) chosen to examine the regional scale relationships between water vapor and SST.

Figure 10. Time series of SST (dashed) and SMMR precipitable water (solid) averaged over the seven regions highlighted on Fig. 9.

Figure 11. Time series of SMMR precipitable water (heavy solid) and the precipitable water predicted from the annually averaged relationship presented in Fig. 6 (thin solid line, middle curve) for the seven selected regions. The shading within the two outer thin lines represents the extent of a standard deviation above and below the predicted water vapor.

Figure 12a. The DJF climatological distribution of $(w - \bar{w})/w$ over the SMMR ocean grid. All DJF seasons of the data set were used in deriving this climatology. Contours are unitless but when multiplied by 100 are the percentage deviation of the predicted water vapor from that observed.

Figure 12b. Same as for Fig. 12b but for JJA averaged.

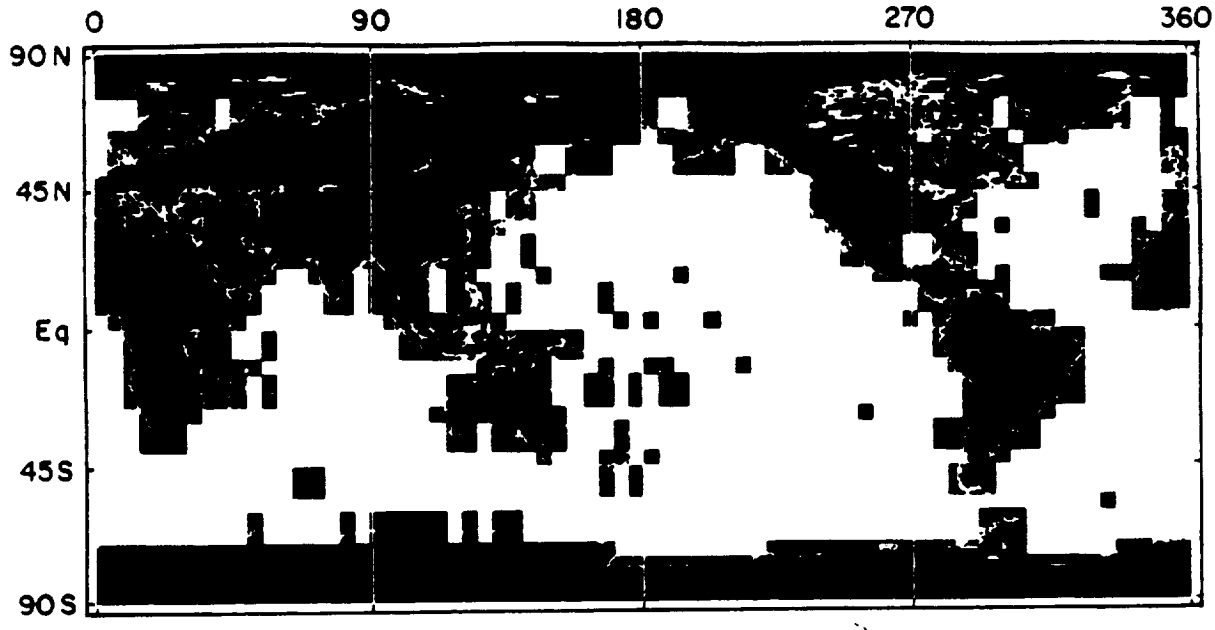

Fig. 1

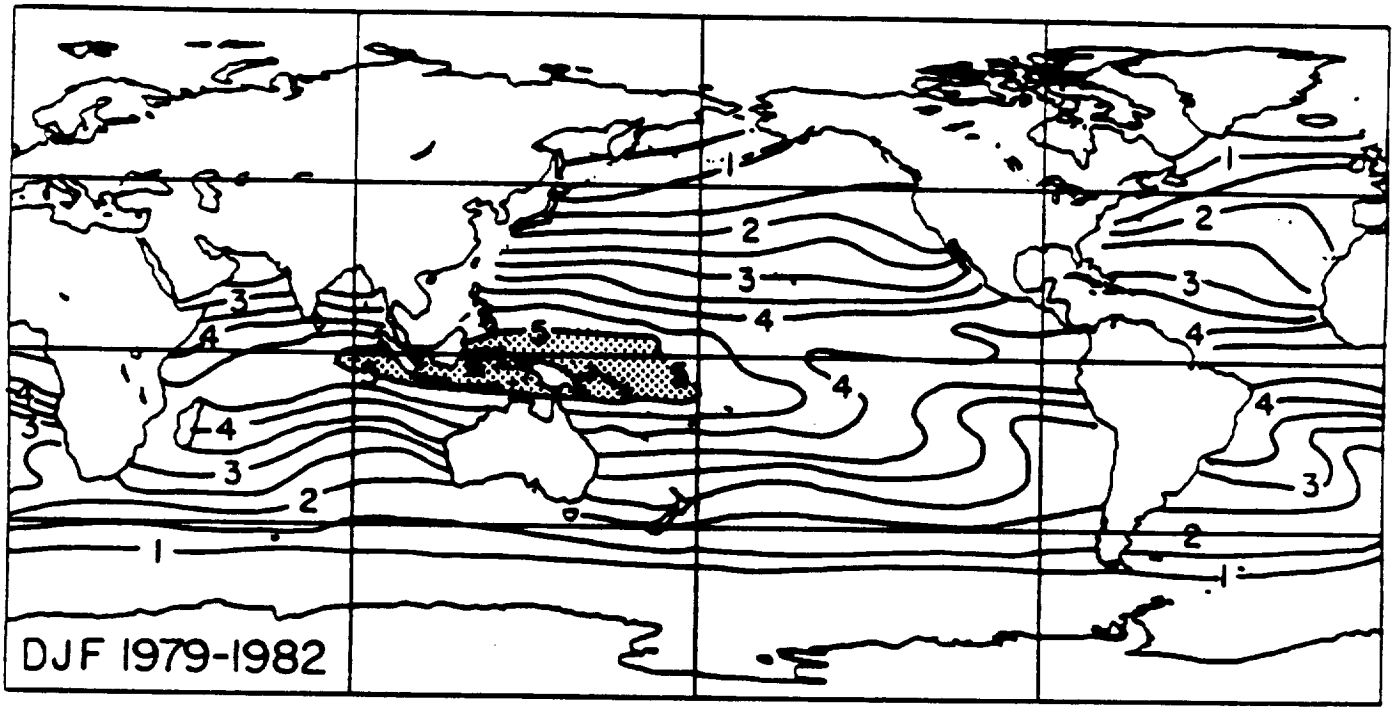

Fig. 2a

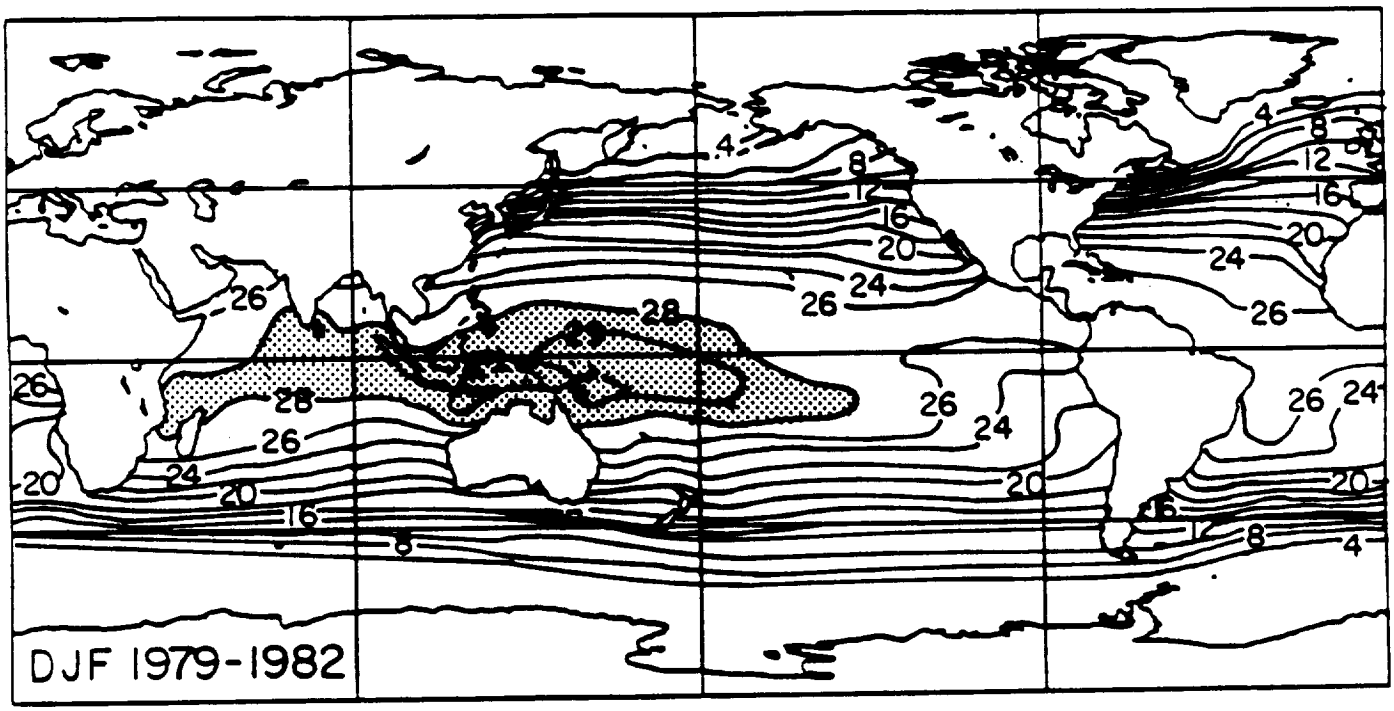

Fig. 25

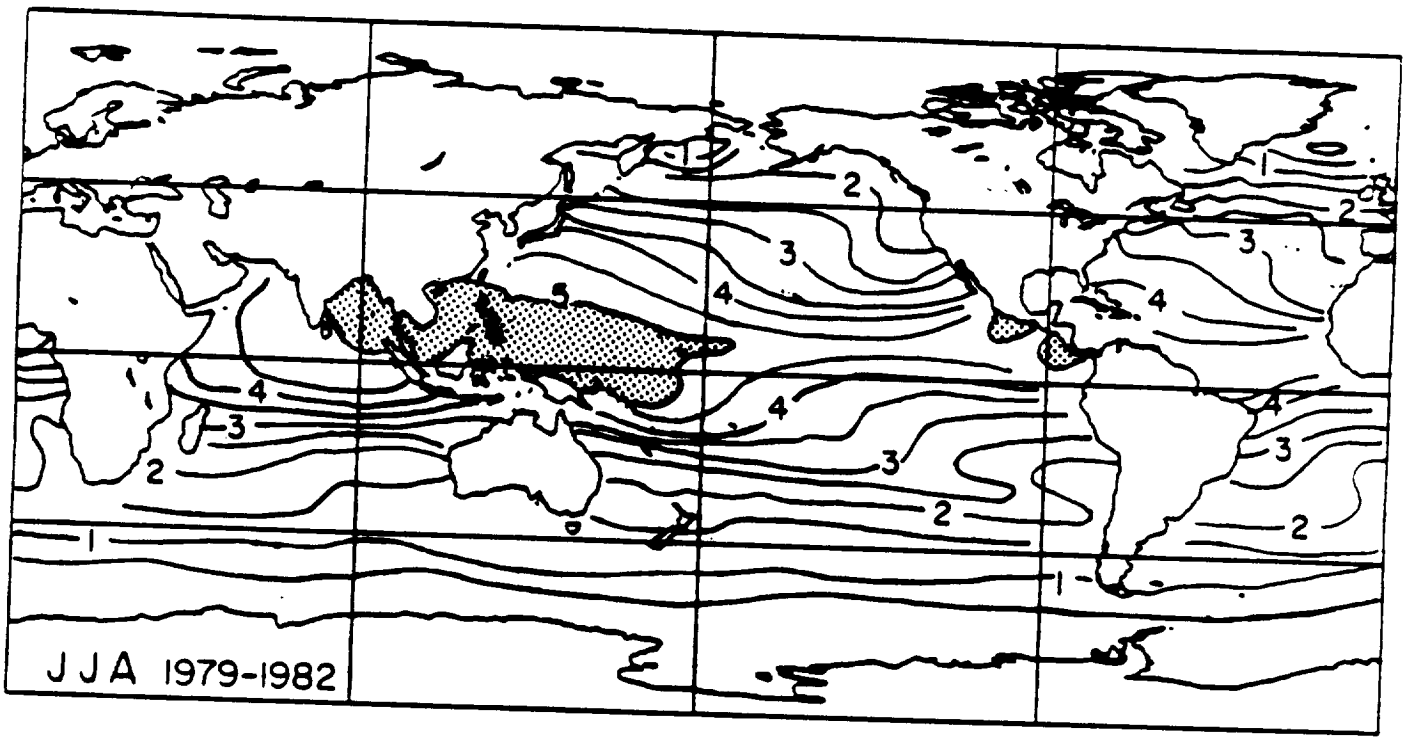

Fig. 3a

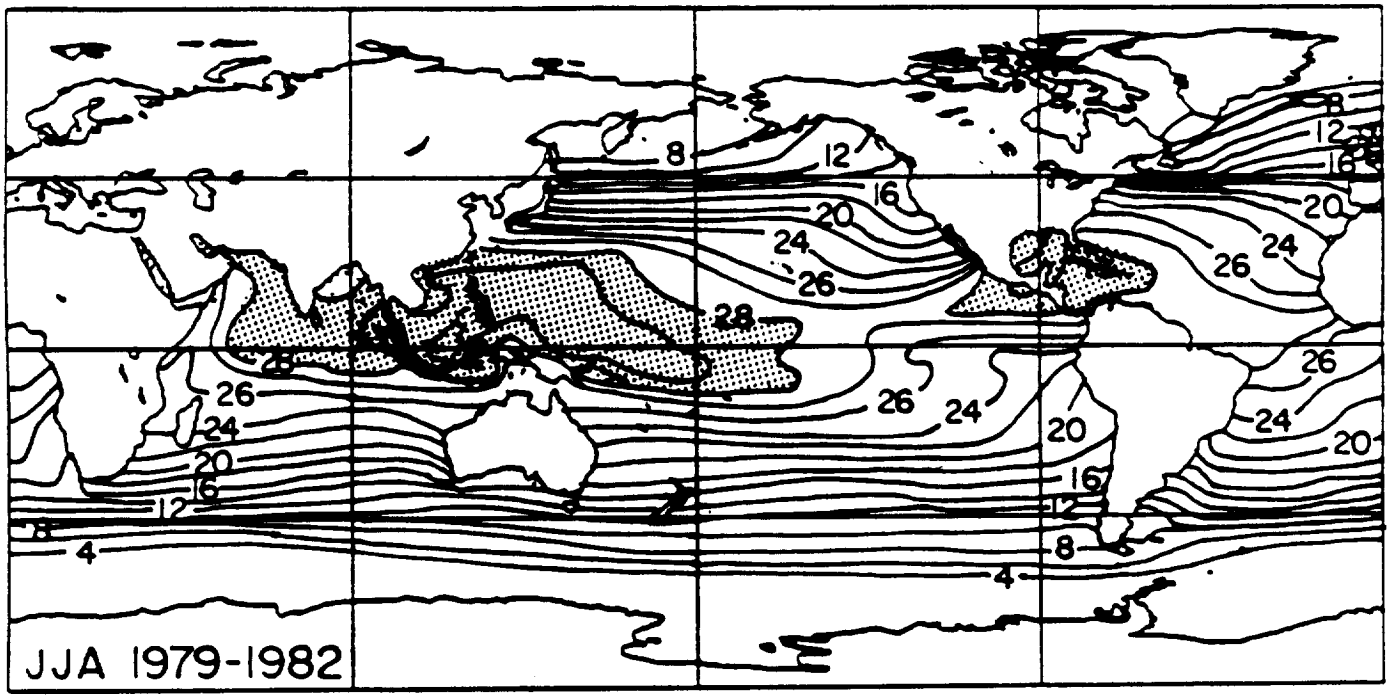

Fig. 3b

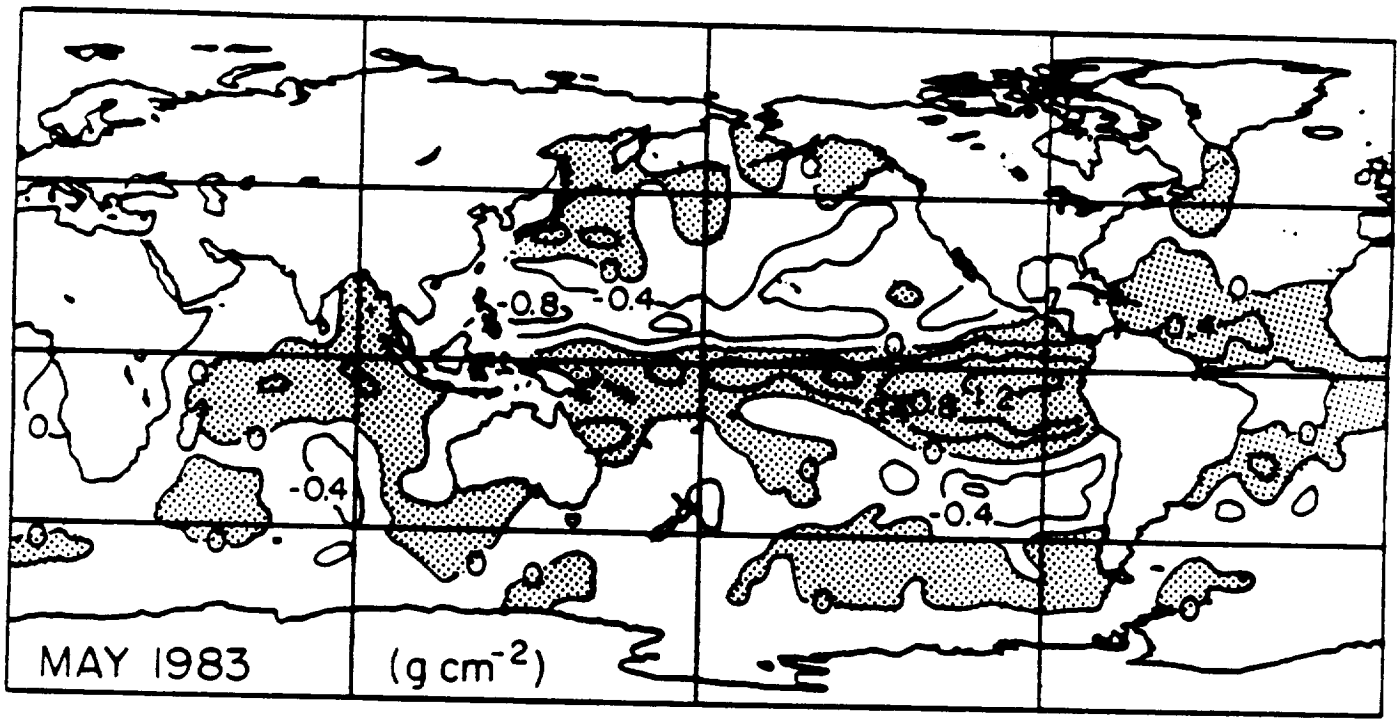

Fig. 4a

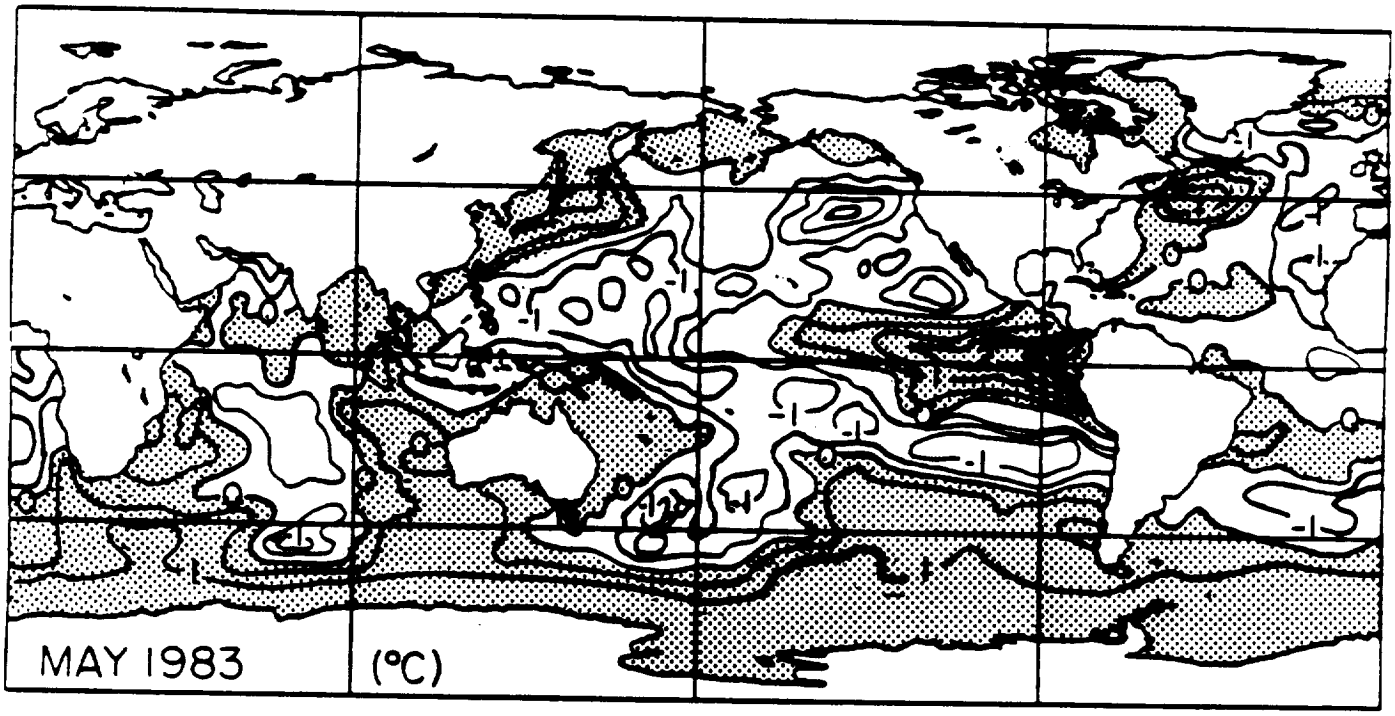

Fig. 4b

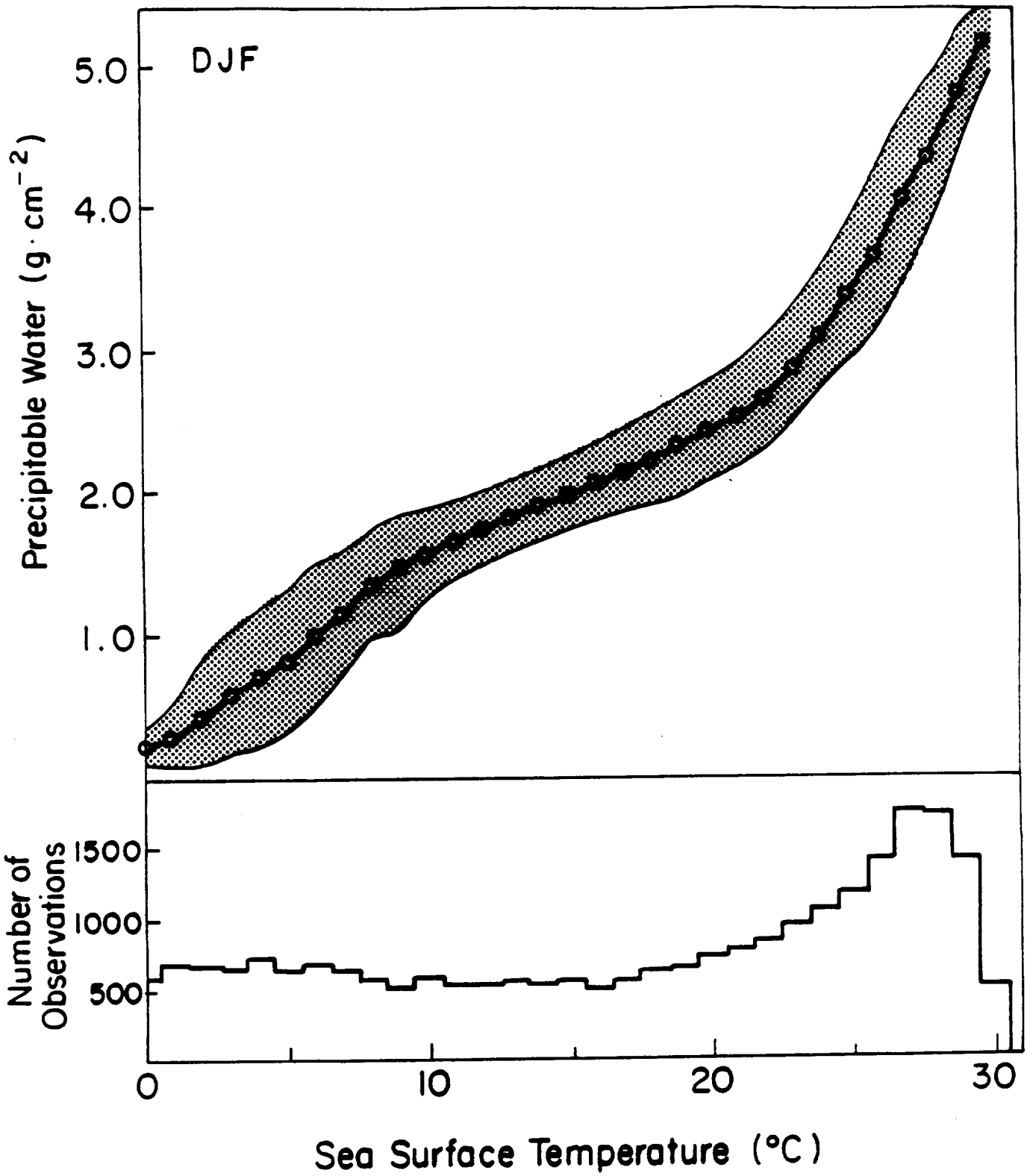
DJF
5.0
4.0
3.0
2.0
1.0
Precipitable Water (g·cm⁻²)
1500
1000
500
Number of Observations
0
10
20
30
Sea Surface Temperature (°C)

Fig. 5a

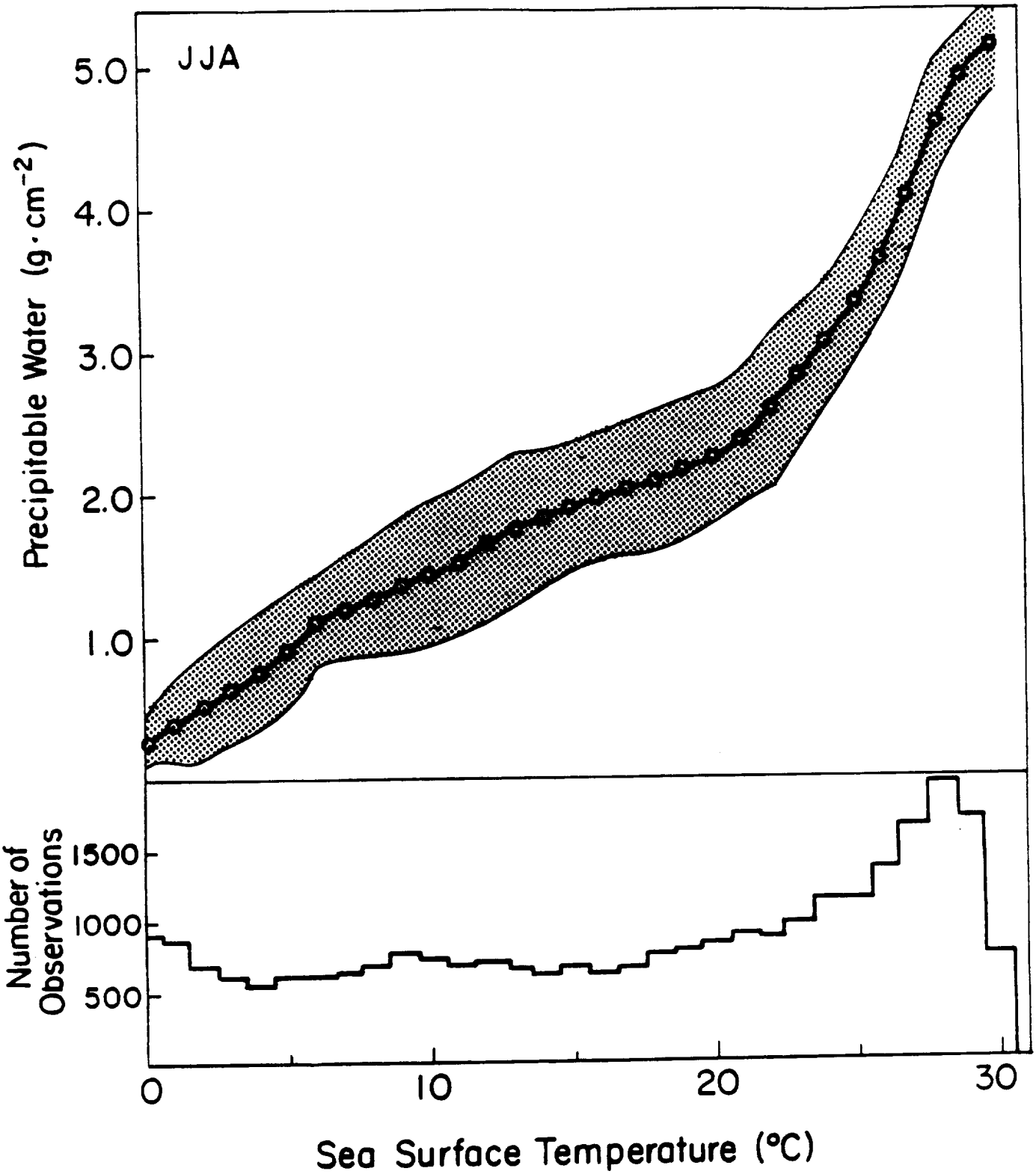
JJA
Precipitable Water (g·cm⁻²)
5.0
4.0
3.0
2.0
1.0
Number of Observations
1500
1000
500
0
10
20
30
Sea Surface Temperature (°C)

Fig. 5b

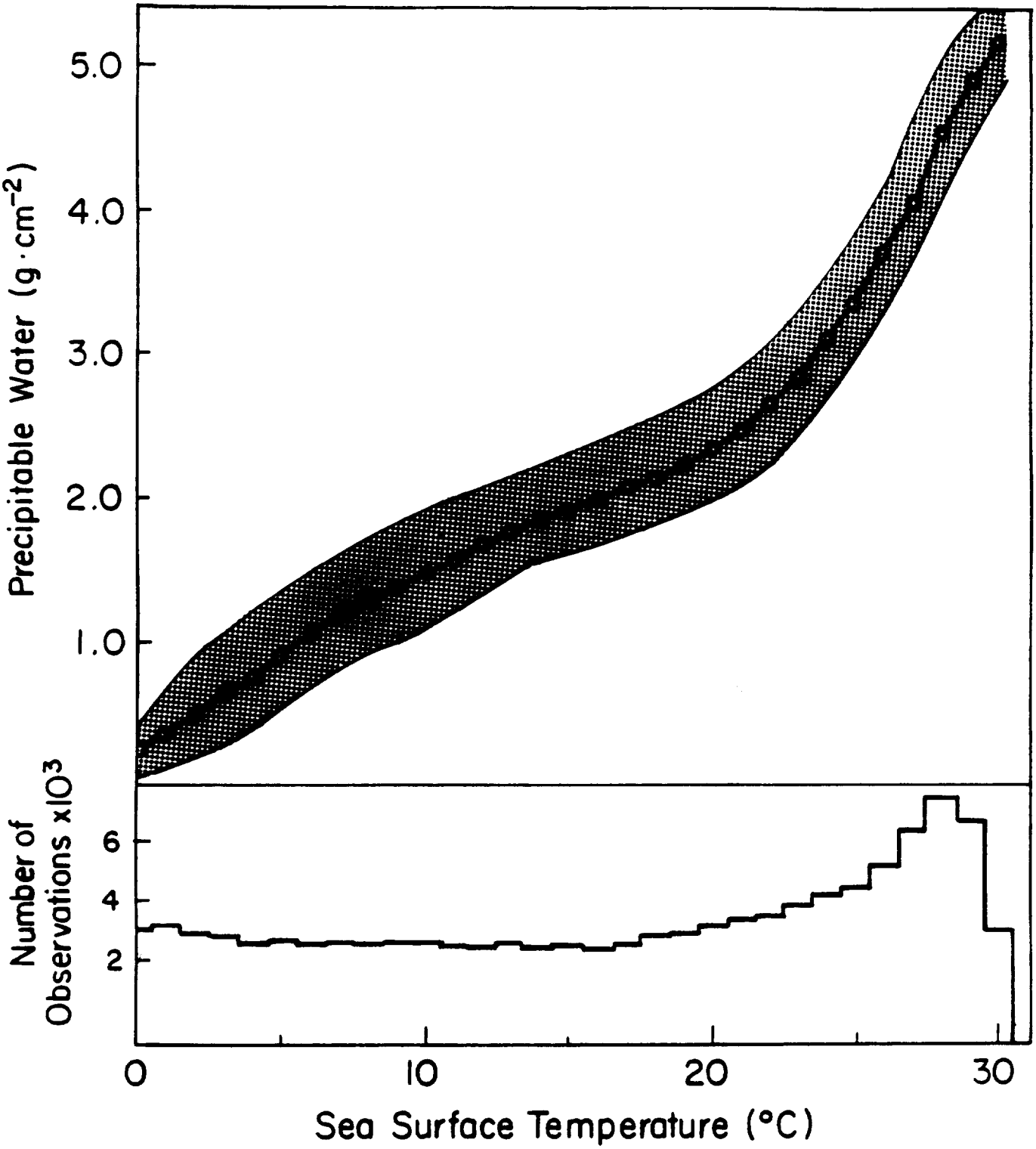
5.0
4.0
3.0
2.0
1.0
Precipitable Water (g·cm⁻²)
Number of Observations x10³
6
4
2
0
10
20
30
Sea Surface Temperature (°C)

Fig. 6

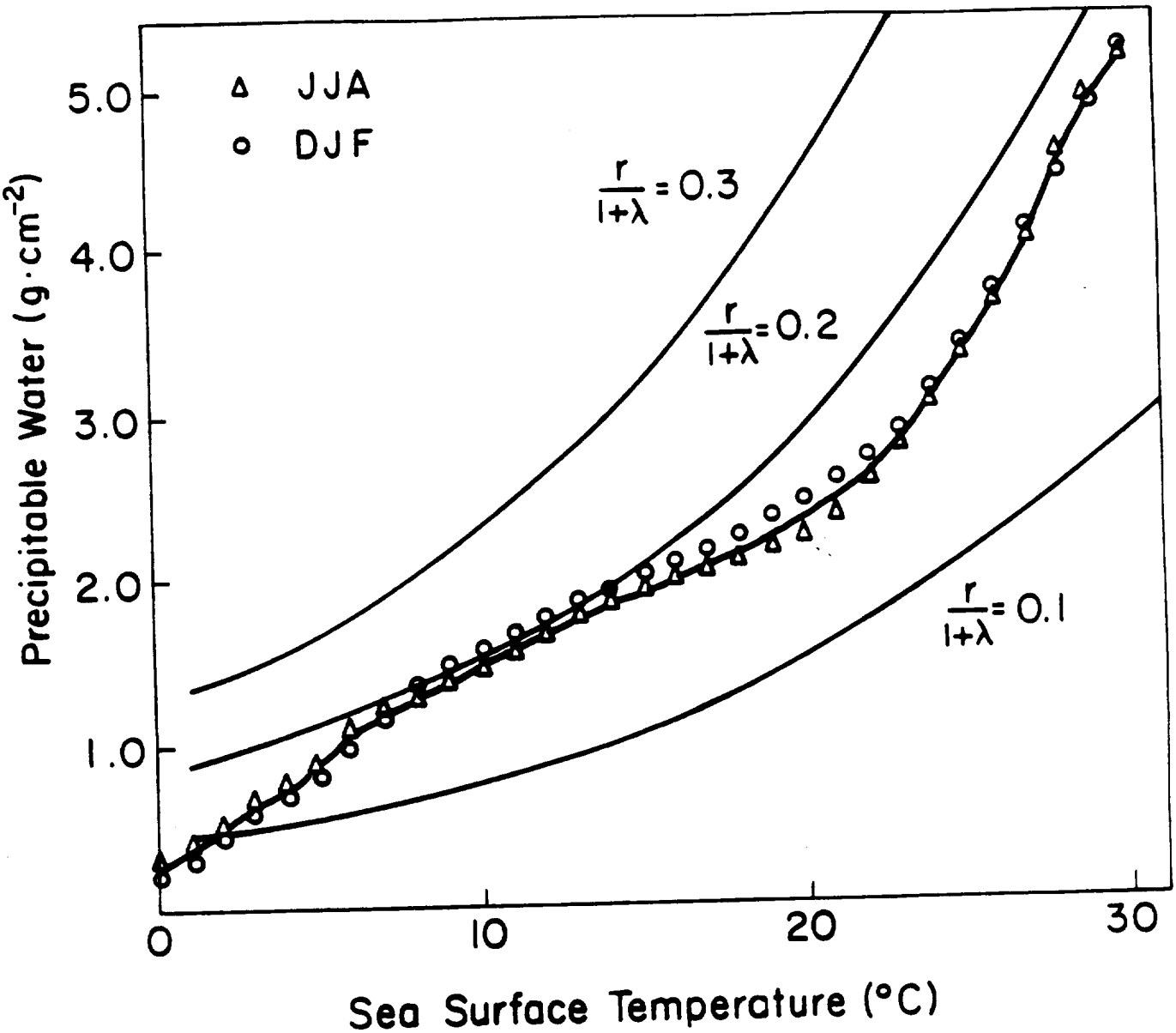
Δ JJA
o DJF
r/(1+λ) = 0.3
r/(1+λ) = 0.2
r/(1+λ) = 0.1
Precipitable Water (g·cm⁻²)
5.0
4.0
3.0
2.0
1.0
0
10
20
30
Sea Surface Temperature (°C)

Fig. 7

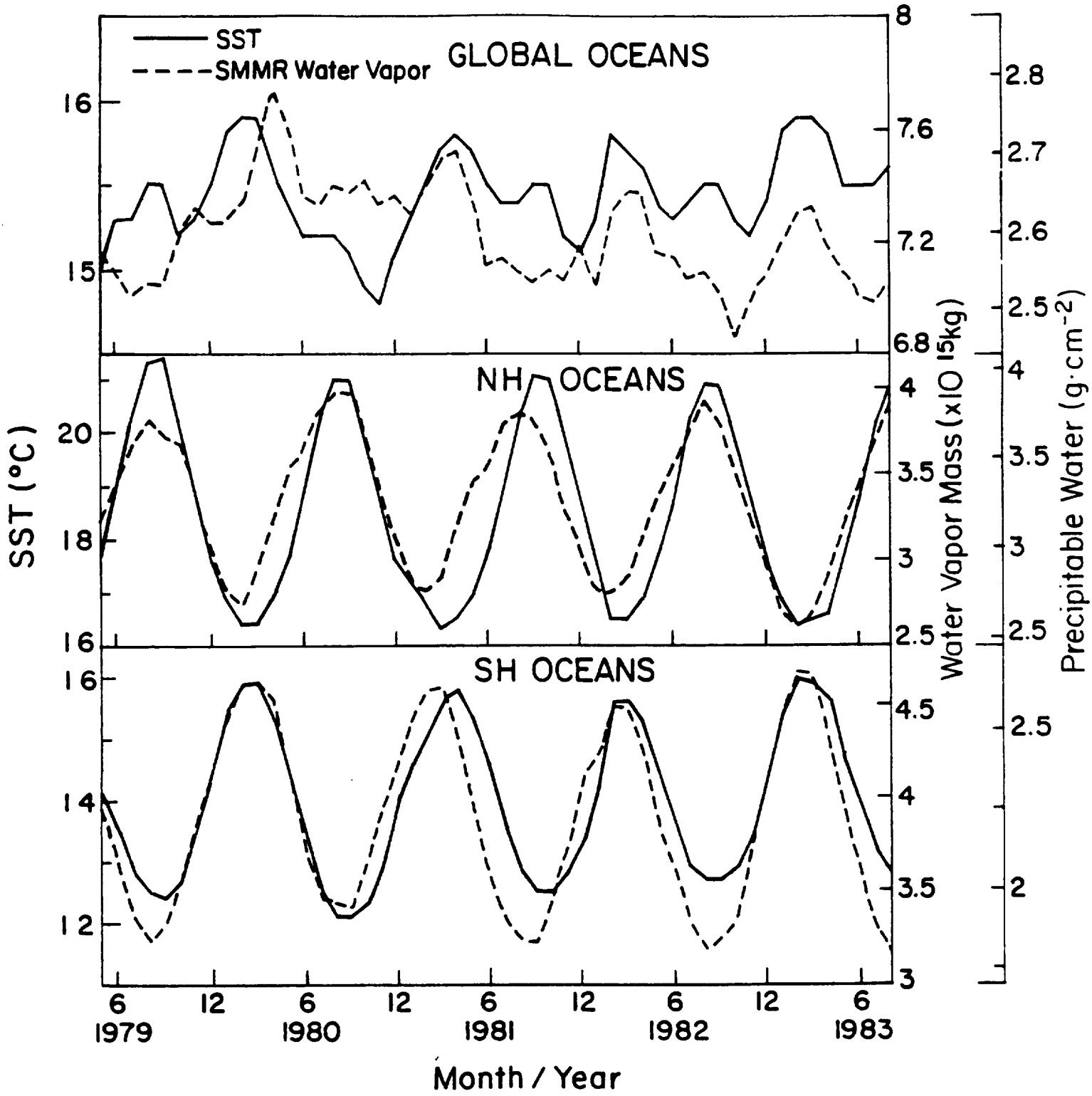
SST
SMMR Water Vapor
GLOBAL OCEANS
NH OCEANS
SH OCEANS
SST (°C)
Water Vapor Mass (x10 15kg)
Precipitable Water (g·cm-2)
Month / Year
1979
1980
1981
1982
1983

Fig. 8

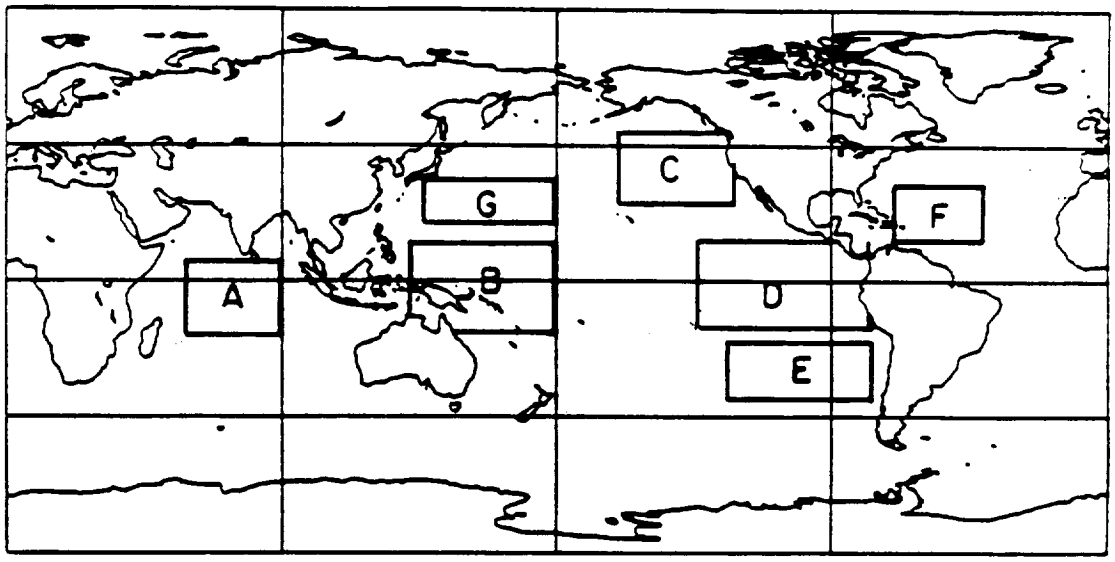

Fig. 9

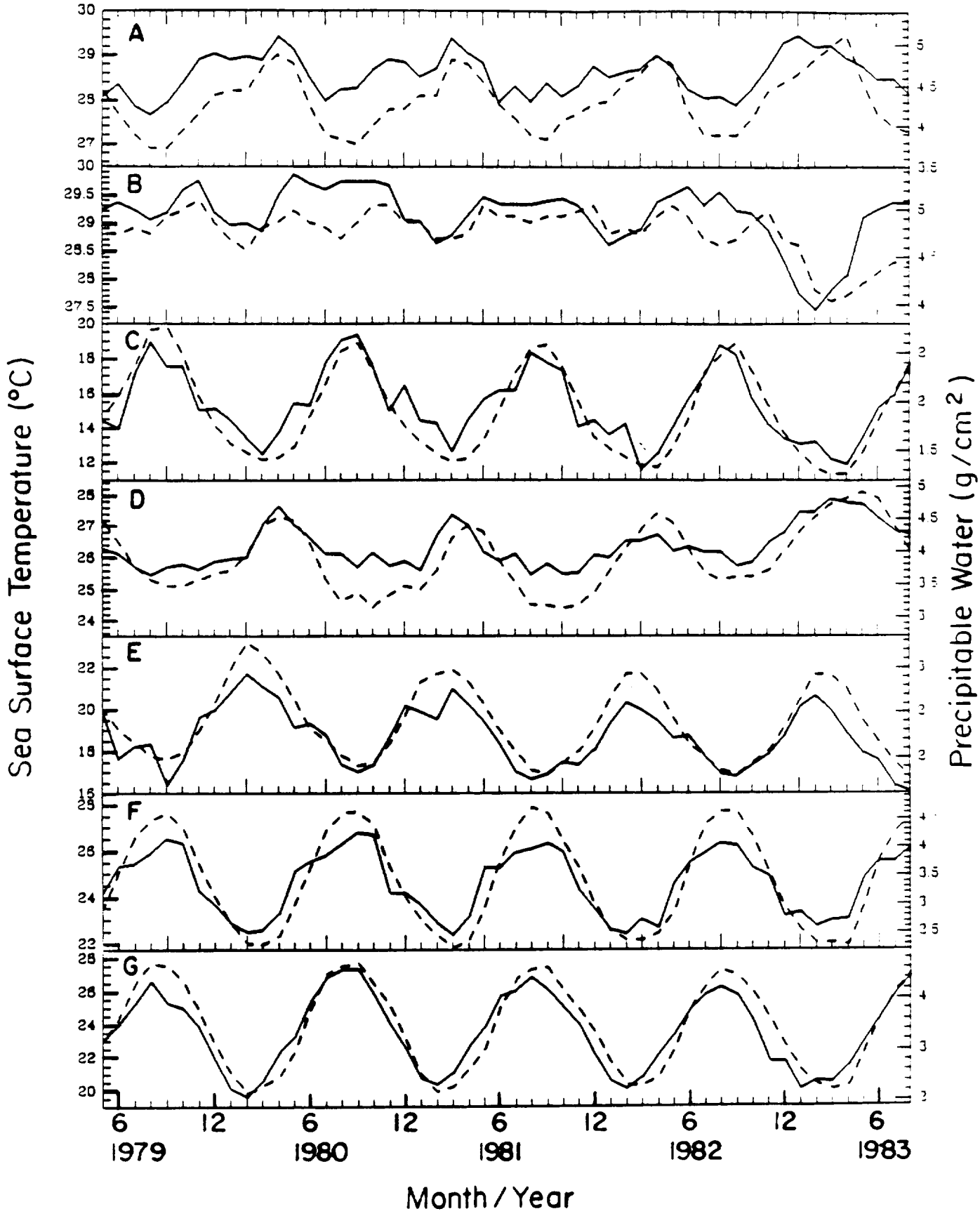
A
B
C
D
E
F
G
Sea Surface Temperature (°C)
Precipitable Water (g/cm²)
6
12
6
12
6
12
6
12
6
1979
1980
1981
1982
1983
Month / Year

Fig. 10

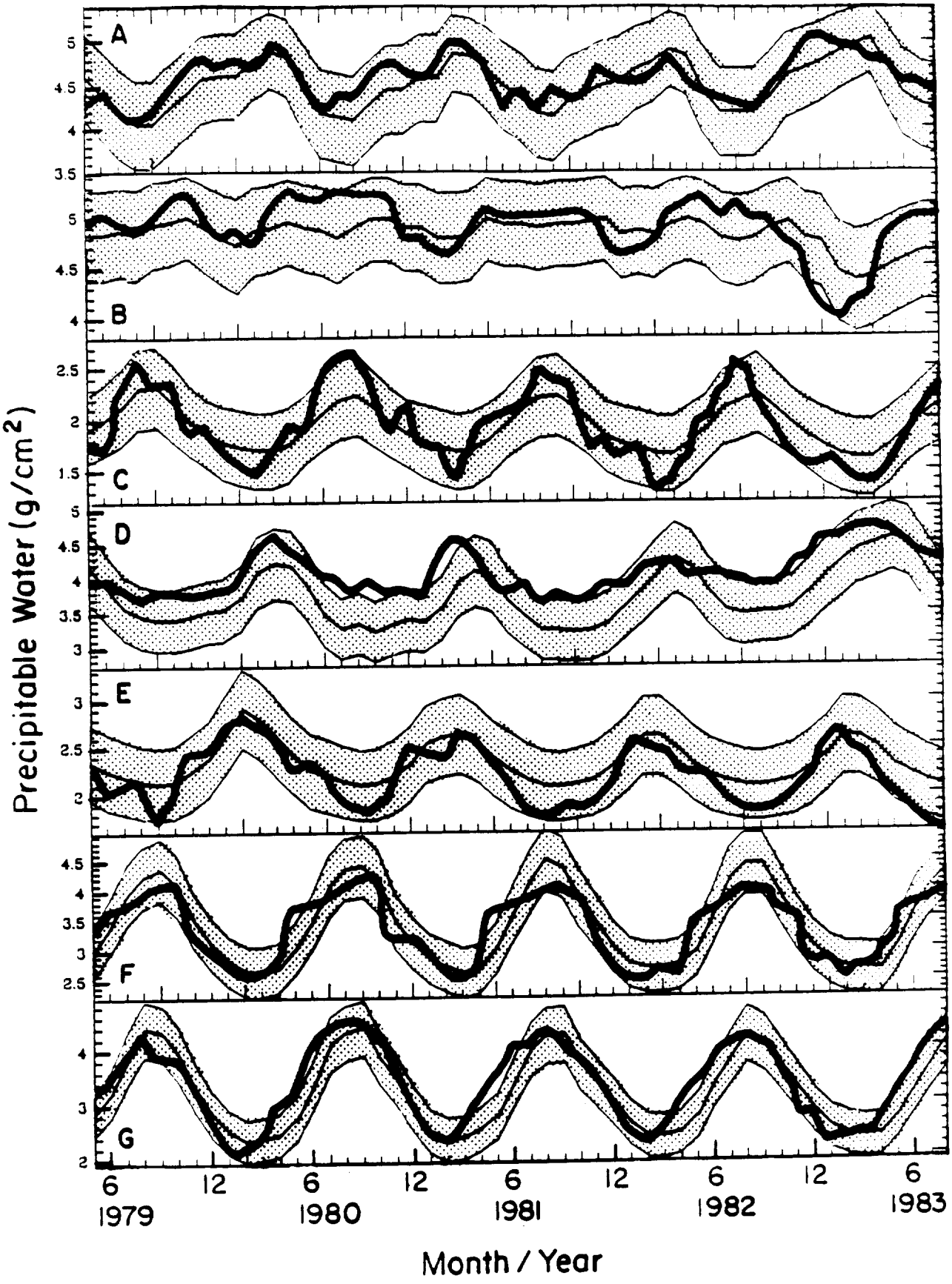
A
B
C
D
E
F
G
Precipitable Water (g/cm²)
6
12
6
12
6
12
6
12
6
1979
1980
1981
1982
1983
Month / Year

Fig. 11

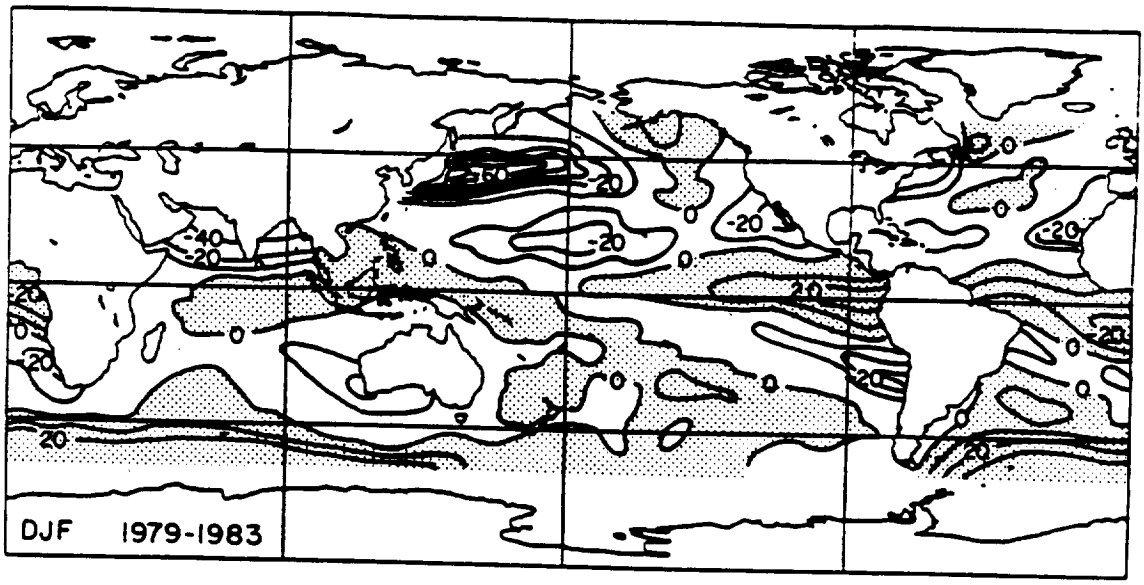

Fig. 12a

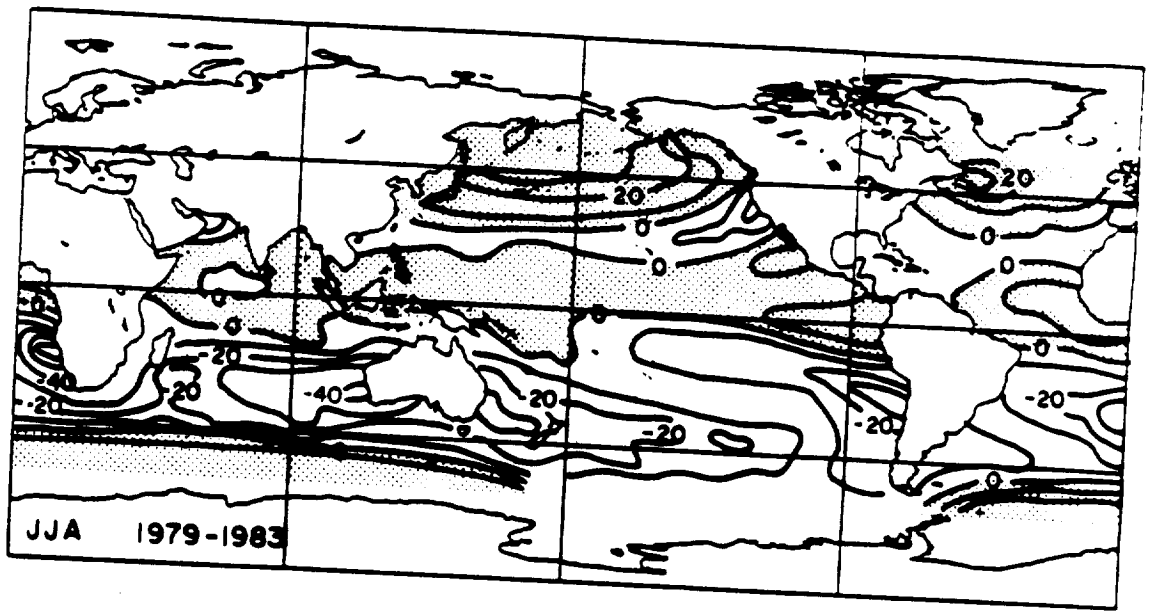

Fig. 12b